Journal of Alloys and Compounds 480 (2009) 696–701

Contents lists available at ScienceDirect

Journal of Alloys and Compounds

journal homepage: www.elsevier.com/locate/jallcom

Properties of $LiNi_{1/3}Co_{1/3}Mn_{1/3}O_2$ cathode material synthesized by a modified Pechini method for high-power lithium-ion batteries

Hui Xia, Hailong Wang, Wei Xiao, Li Lu*, M.O. Lai

Department of Mechanical Engineering, National University of Singapore, 9 Engineering Drive 1, Singapore 117576, Singapore

ARTICLE INFO

Article history:
Received 15 December 2008
Received in revised form 4 February 2009
Accepted 7 February 2009
Available online 20 February 2009

Keywords:
Lithium-ion batteries
Layered compounds
$LiNi_{1/3}Co_{1/3}Mn_{1/3}O_2$
Pechini method
Cathode

ABSTRACT

Layered nano-structured $LiNi_{1/3}Co_{1/3}Mn_{1/3}O_2$ cathode materials were synthesized in air by a modified Pechini method. The crystal structure and surface morphology of the samples were investigated by X-ray diffraction (XRD) and field emission scanning electron microscopy (FESEM). It was found that Li/Ni disorder and particle size of the samples are highly dependent on the synthesis temperature. Magnetic properties of the samples were investigated by SQUID magnetometry to further study the cation disorder of the material. The electrochemical properties of the $LiNi_{1/3}Co_{1/3}Mn_{1/3}O_2$/Li cells were investigated by charge/discharge measurements at different *C* rates. Although the samples synthesized at low temperatures are composed of nano-sized particles, the reversible capacity is relatively low due to the high degree of Li/Ni disorder. The cycle performance of the samples improves as the synthesis temperature increases probably due to the decreased surface area and improved structural stability. The rate capability of the samples depends on both particle size and Li/Ni disorder. The sample synthesized at 900 °C with relative small particle size and low degree Li/Ni disorder exhibited the best rate capability.

1. Introduction

$LiCoO_2$ is the most commonly used cathode material for the commercial lithium-ion batteries [1,2]. However, due to its high cost, toxicity and safety issues at high voltage, further application using $LiCoO_2$ electrode material for large scale batteries has been found to be limited. Therefore, extensive research has been carried out to study and develop alternative cathode materials to replace $LiCoO_2$. Only recently, layered di- and tri-transition metal oxides have become the promising new electrode materials for the next generation lithium-ion batteries [3–6]. Among them, $LiNi_{1/3}Co_{1/3}Mn_{1/3}O_2$ is particularly interesting due to its high reversible capacity, lower cost, less toxicity and enhanced safety features compared to conventional $LiCoO_2$ [5,6]. As shown in Fig. 1, the ideal layered structure of $LiNi_{1/3}Co_{1/3}Mn_{1/3}O_2$, which is nearly a cubic close-packed arrangement of oxygen ions with lithium and transition metal ions occupying alternate layers of octahedral sites, is well suitable for the rapid deintercalation and intercalation of lithium ions. However, there is always some extend of cation mixing between lithium ions and transition metal ions in the layered structure (Fig. 1), which reduces the reversible capacity and lithium mobility [7]. Furthermore, the electrochemical properties of the powders are highly dependent on synthesis processes [8,9]. Therefore, a suitable synthesis method needs to be selected to prepare high performance $LiNi_{1/3}Co_{1/3}Mn_{1/3}O_2$ powders.

The development of cathode materials for lithium-ion batteries that provide high energy density at fast discharge rates is important to meet the demands for high power applications such as hybrid electric vehicles and power tools. It is promising to use nano-particulate cathode materials because the lithium ion and electron diffusion distances within the particles can be greatly reduced and hence improving the power. However, $LiNi_{1/3}Co_{1/3}Mn_{1/3}O_2$ powder prepared by conventional solid-state method often results in an inhomogeneous or impurity with inferior electrochemical performance. Therefore, new methods, such as glycine-nitrate combustion [10], hydroxide co-precipitation [11], solution spray drying [8], sol–gel process [7], molten salt [12], etc., have been developed to prepare high quality $LiNi_{1/3}Co_{1/3}Mn_{1/3}O_2$ powders. Kunduraci and Amatucci [13] successfully prepared nano-structured spinel $LiNi_{1/3}Mn_{2/3}O_4$ cathode materials by a modified Pechini method. The nano-structured $LiNi_{1/3}Mn_{2/3}O_4$ powders exhibited excellent rate capability due to their small particle size.

In this work, $LiNi_{1/3}Co_{1/3}Mn_{1/3}O_2$ powders with different particle sizes were prepared by a modified Pechini method. The influence of synthesis temperature on the particle morphology and crystal structure was investigated. The cation mixing in the samples synthesized at different conditions was also investigated by SQUID measurements. The electrochemical properties of the $LiNi_{1/3}Co_{1/3}Mn_{1/3}O_2$ samples were studied by charge/discharge measurements in half cells.

* Corresponding author. Fax: +65 6779 1459.
E-mail address: mpeluli@nus.edu.sg (L. Lu).

0925-8388/$ – see front matter © 2009 Elsevier B.V. All rights reserved.
doi:10.1016/j.jallcom.2009.02.023

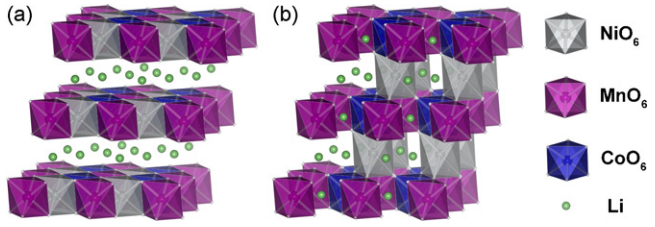

Fig. 1. (a) Ideal layered α-$NaFeO_2$ structure of $LiNi_{1/3}Co_{1/3}Mn_{1/3}O_2$ without Li/Ni intermixing and (b) layered α-$NaFeO_2$ structure of $LiNi_{1/3}Co_{1/3}Mn_{1/3}O_2$ with a high content of Li/Ni intermixing.

2. Experimental

The layered $LiNi_{1/3}Co_{1/3}Mn_{1/3}O_2$ compound was synthesized by a modified Pechini method. The stoichiometric amounts of $LiNO_3$, $Mn(NO_3)_2$ (a solution of 50 wt.% of $Mn(NO_3)_2$ in water), $Co(NO_3)_2{\cdot}6H_2O$ and $Ni(NO_3)_2{\cdot}6H_2O$ were dissolved in deionized water and added dropwise to citric acid-ethylene glycol aqueous solution. The detailed Pechini process can be found in Kunduraci and Amatucci's paper [13]. The final dried product was ground and pressed into pellets. These pellets were heated in a furnace at 400 °C for 4 h, followed by calcination at different temperatures of 700, 800, 900 and 1000 °C for 12 h to obtain $LiNi_{1/3}Co_{1/3}Mn_{1/3}O_2$.

The structure and crystallinity of the samples were characterized using a Shimadzu XRD-6000 X-ray diffractometer with Cu Kα radiation at a scan rate of 1°/min. Profile refinement of the XRD data was carried out using Fullprof to acquire structural information such as lattice parameter and Li/Ni intermixing. The surface morphology and particle size of the samples were investigated by field emission scanning electron microscopy (FESEM). The dependence of the magnetization upon the applied field was measured using a SQUID magnetometer at temperature of 10 K.

To evaluate electrochemical performance, composite electrodes were made by mixing the $LiNi_{1/3}Co_{1/3}Mn_{1/3}O_2$ active material, polytetrafluoroethylene (PTFE) binder and super S carbon with a weight ratio of 80:10:10. Electrochemical measurements were carried out using a Solartron 1287 cell test system with Laboratory made Swagelok cells. The electrochemical cell consisted of a lithium foil as the counter electrode, a composite electrode as the working electrode and 1 M $LiPF_6$ in ethyl carbonate/dimethyl carbonate solution (EC/DEC, 1/1 vol.% OZARK Fluorine Specialities, Inc.) as the electrolyte. Galvanostatic charge/discharge tests were performed on the $Li/LiNi_{1/3}Co_{1/3}Mn_{1/3}O_2$ cells in the voltage window between 2.5 and 4.5 V at different *C* rates, where 1*C* rate is defined as being equal to discharge of the theoretical capacity 280 mAh/g in 1 h.

3. Results

3.1. Structure characterization

The structures of the $LiNi_{1/3}Co_{1/3}Mn_{1/3}O_2$ samples synthesized by Pechini method at different temperatures (700–1000 °C) are shown in Fig. 2. All reflection peaks for each XRD spectrum can be indexed based on a hexagonal α-$NaFeO_2$ structure with a space

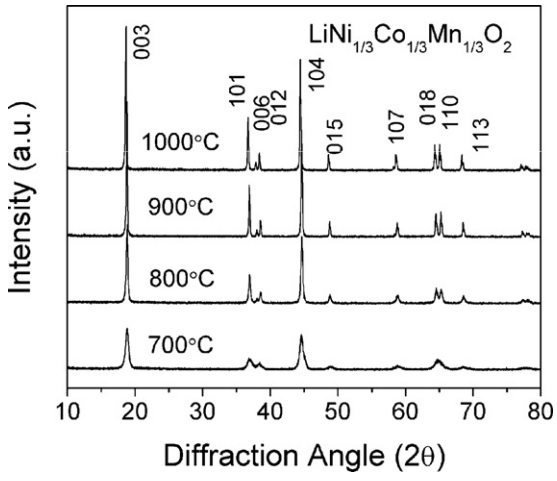

Fig. 2. XRD spectra of $LiNi_{1/3}Co_{1/3}Mn_{1/3}O_2$ powders prepared by Pechini method at different synthesis temperatures.

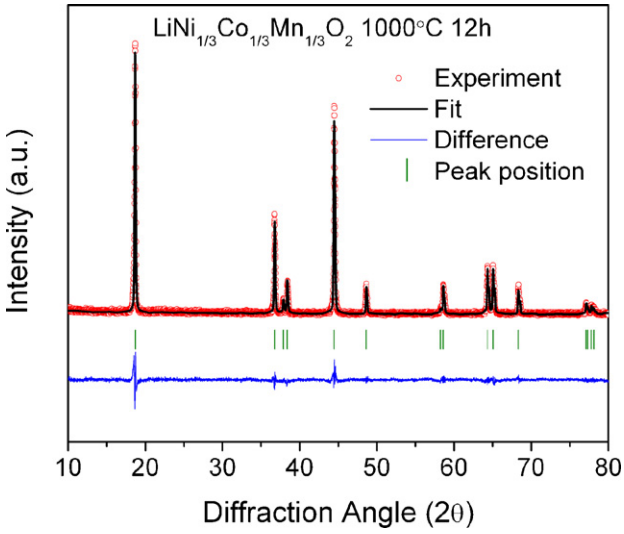

Fig. 3. Rietveld refinement using the XRD spectrum of $LiNi_{1/3}Co_{1/3}Mn_{1/3}O_2$ synthesized at 1000 °C by Fullprof. The structural parameters are given in Table 1.

group *R*3-*m*, indicating phase-pure compound synthesized at different temperatures using Pechini method. The XRD spectrum of the sample synthesized at 700 °C exhibits relatively broad peaks indicating extremely fine crystallite size and low crystallinity. The XRD peaks become sharp and well-defined when the synthesis temperature is above 800 °C, indicating the well-crystallized compound. The clear splitting of the peaks assigned to the Miller indices (0 0 6/0 1 2) and (0 1 8/1 1 0) for the XRD spectra of samples synthesized above 800 °C indicates the particular characteristics of the layered structure. From previous studies on the layered cathode materials, it is well-known that a partial interchange of occupancy of Li and transition metal ions would give rise to cation mixing (disorder) [14]. To investigate the cation intermixing and determine the lattice parameters of the powders synthesized using the Pechini method, Rietveld profile fitting was carried out for each sample using Fullprof. Only partial interchange between Li^+ and Ni^{2+} was considered in the fitting since Co^{3+} and Mn^{4+} can hardly interchange with Li^+ [15]. The experimental XRD spectrum, the calculated XRD spectrum, and the difference between the two spectra of the samples synthesized at 1000 °C are shown in Fig. 3. The refinement results are summarized in Table 1. It can be seen that the structure of the samples is highly dependent on the synthesis temperature. As the synthesis temperature increases from 700 to 1000 °C, the *a*-lattice parameter decreases first from 2.8643 to 2.8623 Å, and then keeps increasing to 2.8644 Å while the *c*-lattice parameter continuously increases from 14.2267 to 14.2466 Å. As discussed by Kang et al. [16], the increased *c*-lattice parameter for the layered material induces an expanded Li slab space, which will be beneficial to the faster Li motion. The *c*/*a* ratio is an indicator of the cation ordering in the layered structure [17]. The larger the ratio, the lesser the cation disorder is. The samples synthesized at high temperatures exhibit a larger *c*/*a* ratio than the samples synthesized at low temperatures, indicating that a high synthesis temperature is required to achieve a high degree of cation ordering in this material. The cation

Table 1
Rietveld refinement results for the XRD patterns of $LiNi_{1/3}Co_{1/3}Mn_{1/3}O_2$ powders synthesized at different temperatures by Pechini method.

Temperature (°C)	*a* (Å)	*c* (Å)	*c*/*a*	Ni_{3a}	R_{wp} (%)	R_p (%)
700	2.8643(2)	14.2267(26)	4.966	0.101	18.7	14.1
800	2.8623(1)	14.2339(13)	4.972	0.068	18.1	13.6
900	2.8635(1)	14.2456(8)	4.974	0.041	17.7	13.3
1000	2.8644(1)	14.2466(7)	4.973	0.036	17.6	13.1

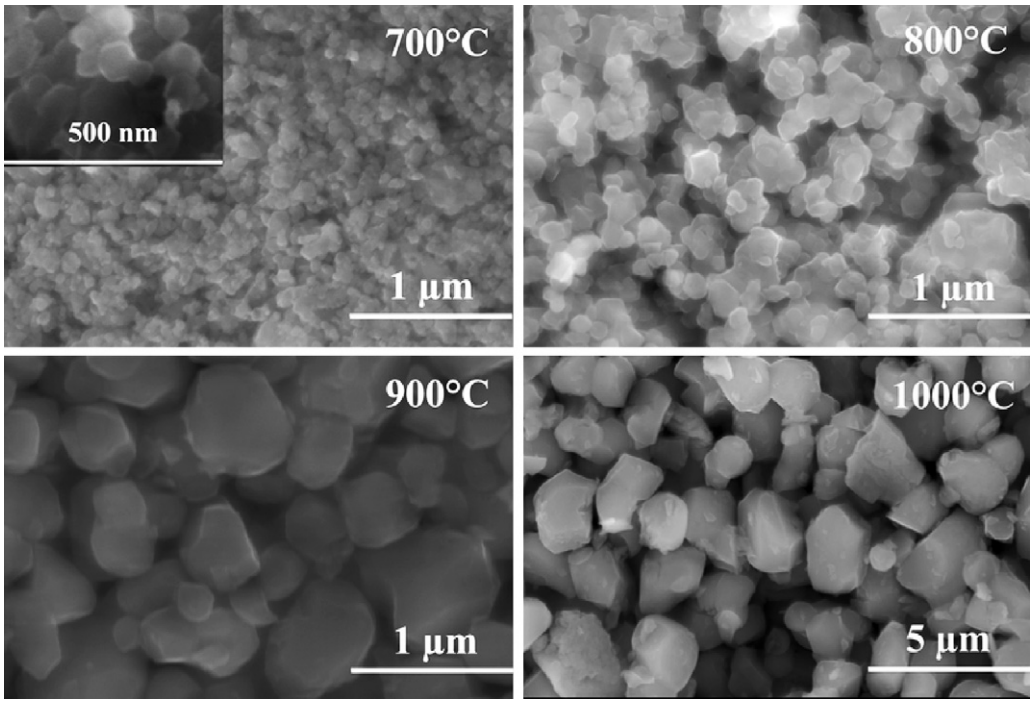

Fig. 4. FESEM images of $LiNi_{1/3}Co_{1/3}Mn_{1/3}O_2$ powders synthesized at different temperatures by Pechini method: (a) 700 °C, (b) 800 °C, (c) 900 °C, and (d) 1000 °C.

disorder of about 10% Ni ions present in the Li layer is extremely high for the sample synthesized at 700 °C. As the synthesis temperature increases, the cation disorder decreases and a relatively low Li^+–Ni^{2+} intermixing of 3–4% can be achieved for the samples synthesized at 900 and 1000 °C.

3.2. Surface morphology

The morphology of the samples was examined using FESEM as shown in Fig. 4. It can be seen that the primary particle size of the samples is highly dependent on the synthesis temperature. The sample calcinated at 700 °C is composed of very uniform and small nano-crystallites with particle size about 50 nm. As the synthesis temperature increases, the 800, 900 and 1000 °C produced samples show increased particle sizes of about 100–200 nm, 0.5–1 μm and 2–3 μm, respectively. Well-defined particles with hexagonal shapes are formed for all the samples, indicating a layered structure of the $LiNi_{1/3}Co_{1/3}Mn_{1/3}O_2$ compound synthesized at all temperatures. The merit of the Pechini method is that ultra fine particles of the $LiNi_{1/3}Co_{1/3}Mn_{1/3}O_2$ compound can be synthesized at relatively low calcination temperature. The samples synthesized at 700 and 800 °C seem very promising for high-power lithium-ion batteries because their nano-sized particles can greatly reduce the diffusion paths for Li ions.

3.3. Magnetic properties

It has been reported that the existence of Ni^{2+} ions in the Li layer can strongly affect magnetic properties of layered compounds [18]. For the layered $LiNi_{1/2}Mn_{1/2}O_2$ compound, a hysteresis loop with a remnant magnetization can be observed for the magnetization measurements [19,20]. The magnetic order was believed to be induced by the formation of magnetic clusters around the Ni^{2+} ions in the Li layer. The net magnetization in the $LiNi_{1/2}Mn_{1/2}O_2$ is speculated to be due to the antiferromagnetic interaction of 180° Ni^{2+} (3a)–O–Ni^{2+} (3b) bonds by Chernova et al. [19]. While Abdel-Ghany et al. [20] attributed the long-range magnetic ordering in $LiNi_{1/2}Mn_{1/2}O_2$ to the ferromagnetic interaction of 180° Ni^{2+}(3a) –O–Mn^{4+}(3b) bonds. When Co is added to the $LiNi_{1/2}Mn_{1/2}O_2$ compound, the hysteresis loop is much less pronounced with reduced remanent magnetization and coercivity. In the Co-containing compound, the increase of Co content leads to a dilution of the magnetic transition metal layers with non-magnetic Co^{3+} ions and Co is known to reduce the migration of Ni ions to Li layers [21]. The magnetization curves of the $LiNi_{1/3}Co_{1/3}Mn_{1/3}O_2$ samples are shown in Fig. 5. The sample synthesized at 700 °C shows a relatively more pronounced hysteresis loop with a larger remnant magnetization and coercivity. All other samples show minimal hysteresis loops, which indicate that a relatively larger amount of Ni^{2+} ions exists in the Li layer in the sample synthesized at 700 °C confirming the highest disordering of the sample synthesized at 700 °C as predicted by the Rietveld refinement.

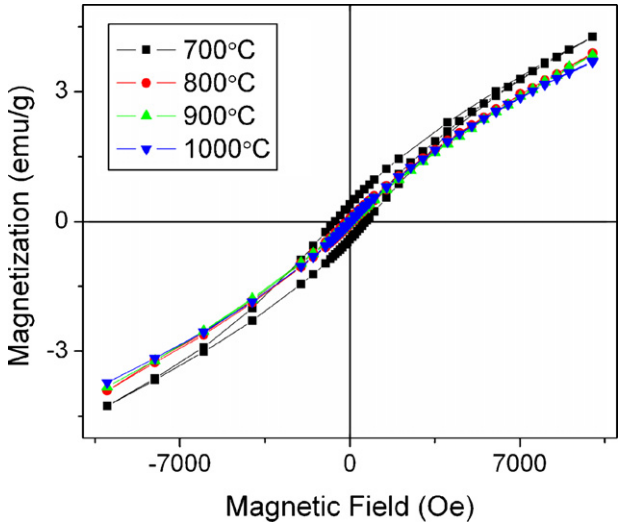

Fig. 5. The magnetization curves of the $LiNi_{1/3}Co_{1/3}Mn_{1/3}O_2$ powders synthesized at different temperatures.

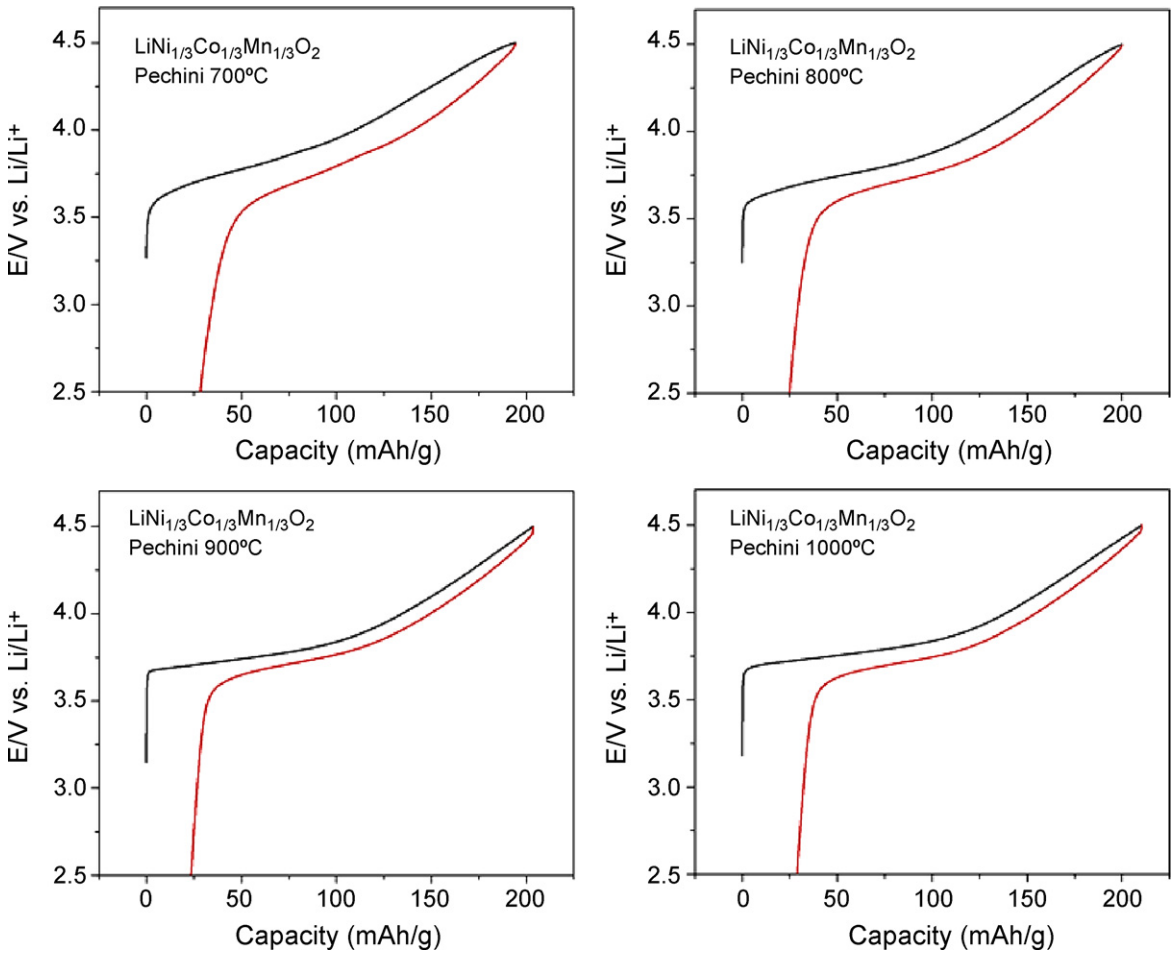

Fig. 6. The first charge/discharge curves of Li/$LiNi_{1/3}Co_{1/3}Mn_{1/3}O_2$ cells using different $LiNi_{1/3}Co_{1/3}Mn_{1/3}O_2$ powders in the voltage window of 2.5–4.5 V at *C*/20 rate.

3.4. Charge–discharge curves

Fig. 6 shows the first charge/discharge curves of different samples between 2.5 and 4.5 V under *C*/20 rate at room temperature. The initial open circuit voltages of the freshly assembled cells were around 3.1 and 3.2 V. On applying the current, the cell voltage rapidly increased to about 3.7 V and then gradually increased until it reached the upper voltage limit of 4.5 V for all the samples. This charge/discharge behavior of Pechini $LiNi_{1/3}Co_{1/3}Mn_{1/3}O_2$ agrees well with the literature reports by other groups [22,23]. It can be seen that the charge/discharge behavior of the $LiNi_{1/3}Co_{1/3}Mn_{1/3}O_2$ is different with that of the layered $LiCoO_2$ which has well-defined plateau at about 3.9 V indicating a first order phase transition [24]. For the $LiNi_{1/3}Co_{1/3}Mn_{1/3}O_2$, existence of Ni ions in the Li layer is believed to anchor the structural framework of the host during Li insertion/extraction and hence leads to improved structural stability [25]. The first cycle charge/discharge capacities and irreversible capacities for different samples are tabulated in Table 2. It can be seen that both charge and discharge capacities increase as the synthesis temperature increases. From the XRD and FESEM results, we know that the sample produced at 700 °C is composed of nano-sized particles with relatively lower degree of crystallization. It is speculated that the structural defects especially at grain boundaries for the low temperature synthesized samples limit the removal of Li ions from the material. As discussed by Bereger et al. [26], the extraction of Li in the transition metal layer happens at very early stage of the charge process for $LiNi_{1/2}Mn_{1/2}O_2$, which will create a vacancy in the transition metal (TM) layer. A vacancy in the TM layer creates two empty tetrahedral sites above and below the TM layer, which will form Li–Li dumbbell if these sites are occupied by Li. The extraction of Li from the tetrahedral sites requires very high potential (>4.6 V). If the same mechanism applies to $LiNi_{1/3}Co_{1/3}Mn_{1/3}O_2$, the increased content of Li in the TM layer in the low temperature synthesized samples will lower the charge capacity with an upper limit of 4.5 V. The samples synthesized at 900 and 1000 °C show large charge/discharge capacities of 203/180 and 210/181 mAh/g, respectively, which agrees well with literature report on well-crystallized $LiNi_{1/3}Co_{1/3}Mn_{1/3}O_2$ with about 4% Li/Ni intermixing [22,23]. The irreversible capacity for the first cycle decreases as the synthesis temperature increases from 700 to 900 °C, then increases as the synthesis temperature goes up to 1000 °C. There are several factors affecting the irreversible capacity of this electrode material. Firstly, in the layered structure, Ni ions in the Li layer can reduce the vacant site available for lithium insertion, and impede lithium motion in the Li layer due to the strong repulsive force between mobile Li ions and fixed Ni ions [16]. Therefore, a larger content of Li/Ni intermixing in this material will lead to a larger irreversible capacity for the first cycle. Secondly, the side reaction between the electrolyte and electrode, and additionally the oxygen release at

Table 2
The first cycle charge–discharge capacities and irreversible capacity loss of $LiNi_{1/3}Co_{1/3}Mn_{1/3}O_2$ prepared by Pechini method.

	700 °C	800 °C	900 °C	1000 °C
First charge (mAh/g)	194	200	203	210
First discharge (mAh/g)	165	175	180	181
Irreversible capacity (%)	14.6	12.5	11.5	13.7

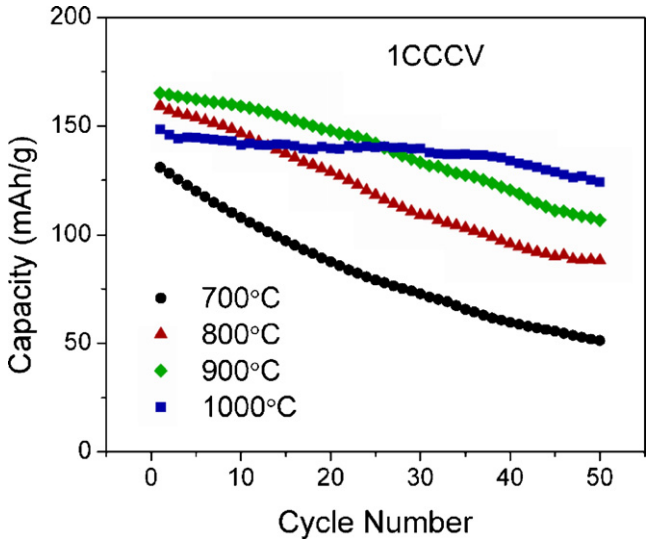

Fig. 7. Cycle performance of Li/$LiNi_{1/3}Co_{1/3}Mn_{1/3}O_2$ cells using different $LiNi_{1/3}Co_{1/3}Mn_{1/3}O_2$ powders in the voltage window of 2.5–4. 5 V at 1*C* rate. (For the charge process, after the cell voltage reaches 4.5 V the cell is hold at 4.5 V for 1 h in the constant-current and constant-voltage (CCCV) mode.)

high voltage may contribute to the irreversible capacity loss for the first cycle [27]. The irreversible capacity loss due to this reason is proportional to the surface area of the electrode. Thirdly, the slow Li in-diffusion for the last Li insertion during the discharge process probably will induce some irreversible capacity loss [21]. The small particle size, high content of Li/Ni intermixing and large surface area for the low temperature synthesized samples therefore lead to a relatively larger irreversible capacity loss. However, nanoparticle size tends to grow to large particle size at high processing temperature, resulting in the increased Li ion diffusion path. As a consequence, the irreversible capacity loss turns to increase as the particle size becomes very big.

3.5. Cycle performance

The cycle performance of $LiNi_{1/3}Co_{1/3}Mn_{1/3}O_2$ electrodes in Swagelok cells within the voltage window of 2.5–4.5 V at 1*C* charge/discharge rate for 50 cycles is shown in Fig. 7. For the charge process, after the cell voltage reaches 4.5 V the cell is held at 4.5 V for 1 h in the constant-current and constant-voltage (CCCV) mode. The initial/final capacities for the samples synthesized at 700, 800, 900, and 1000 °C are 131/51, 159/88, 165/106 and 148/124 mAh/g, respectively. Although the capacity fading was observed for all the samples, the capacity retention is improved as the synthesis temperature increases. Based on the XRD and FESEM results, the samples synthesized at low temperature may not be well-crystallized (such as 700 °C), and the layered structure would not be rigid enough to be maintained upon extensive cycling. Therefore, there is probably structural degradation with cycling for the samples synthesized at low temperature, which would induce a rapid capacity fading. In addition, the side reaction between the electrolyte and the electrode, which would form surface layer, may also contribute to the impedance growth of the cell and lead to capacity fading. The impedance growth due to the formation of surface layer was considered as the main reason for the capacity fading for the layered $LiCoO_2$ electrode when cycled above 4.2 V [28,29]. Therefore, the samples synthesized at low temperature with small particle size and large surface area would probably accelerate the interface reaction between the electrolyte and the electrode, leading to fast capacity fading.

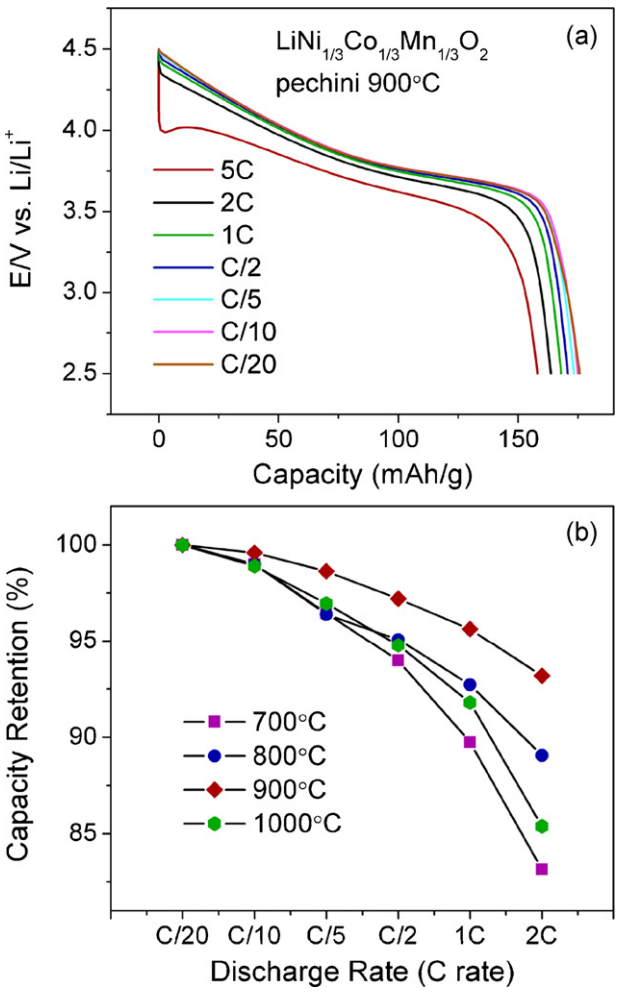

Fig. 8. (a) Discharge curves of a Li/$LiNi_{1/3}Co_{1/3}Mn_{1/3}O_2$ cell at different discharge rates using 900 °C synthesized $LiNi_{1/3}Co_{1/3}Mn_{1/3}O_2$ powders (To do the rate capability test, the cell was charged to 4.5 V using the same *C*/20 rate, then hold at 4.5 V for 1 h, and discharged at different *C* rates.) and (b) percent rate retention of Li/$LiNi_{1/3}Co_{1/3}Mn_{1/3}O_2$ cells using different $LiNi_{1/3}Co_{1/3}Mn_{1/3}O_2$ powders.

3.6. Rate capability

To realize lithium-ion batteries for high power applications, it requires the electrode materials have good rate capability, which means the electrode can maintain a large amount of its full capacity when discharged at a high rate. The rate capabilities of different $LiNi_{1/3}Co_{1/3}Mn_{1/3}O_2$ samples discharged at different *C* rates are shown in Fig. 8. The cell was charged to 4.5 V using the same *C*/20 rate, and then held at 4.5 V for 1 h, followed by discharge at different *C* rates. Fig. 8(a) shows the discharge curves at different C rates for the sample synthesized at 900 °C. It can be seen that the discharge capacity reduces with the increase of the *C* rate. The lowering of discharge curve at high *C* rates is due to the polarization of the cell induced by the cell resistance, which is mainly contributed by the Li ion transport into and through the electrode. Fig. 8(b) shows the percent capacity retention at different discharge rates for different samples. The discharge capacity of the cell at *C*/20 rate was set as 100% of its full capacity. It can be seen that the rate capability of the $LiNi_{1/3}Co_{1/3}Mn_{1/3}O_2$ improves as the synthesis temperature increases from 700 to 900 °C. It is interesting to observe this trend because the nano-sized $LiNi_{1/3}Co_{1/3}Mn_{1/3}O_2$ samples prepared at 700 or 800 °C have much shorter diffusion paths for Li ions and would have better rate performance than the 900 °C produced samples with much bigger particle size. It should be noted that the Li ion

diffusion in this layered material not only depends on the particle size but also depends on the Li ion diffusion barrier which is highly dependent on the structure of this material. The Ni ions in the Li layers would attract oxygen ions from adjacent oxygen layers thereby locally shortening the oxygen–oxygen distance between neighboring MO_2 (M = transition metal ions on 3b layer) slabs, as discussed by Kang et al. [16] for layered $LiNi_{1/2}Mn_{1/2}O_2$. Because the Li ions migrating between two neighboring octahedral sites in the same lithium layer are also required to pass through an empty tetrahedral site, the decrease in the oxygen–oxygen distance would cause an increase in the activation energy for Li ion motion. The first principle calculations [16] show that the activation energy for Li migration is very sensitive to the spacing between oxygen layers. In addition, the Ni ions exist in the Li layers would exert a strong electrostatic repulsion on the Li ions and drastically hamper their reinsertion. The samples synthesized at 700 and 800 °C have a larger content of Li/Ni intermixing and relatively smaller *c*-lattice parameter as shown from the refinement results, which probably induces very high Li diffusion barrier in these less-ordered materials. Therefore the sluggish Li ion diffusion in these low temperature synthesized samples would probably lead to the relatively poor rate capability. However, the trend is not kept when the synthesis temperature is further increased to 1000 °C. It is noticed that the 1000 °C produced samples have very large particle size (2–3 μm) while the Li/Ni intermixing cannot be further reduced (similar to that of 900 °C produced samples). Therefore, the increased Li ion diffusion paths now become the dominant factor which limits the rate capability and leads to the degradation of rate performance of the cell.

4. Conclusions

Phase-pure layered $LiNi_{1/3}Co_{1/3}Mn_{1/3}O_2$ compounds have been successfully synthesized using a modified Pechini method. The structure ordering and particle size of the samples are highly dependent on the synthesis temperature. Although the samples synthesized at low temperature exhibit nano-sized particles, there exists a large amount of cation disorder (Li/Ni intermixing) in the material and crystallization may not be completed. The samples synthesized at high temperature exhibit reduced cation disorder and high degree of crystallization. The electrochemical performance of Pechini $LiNi_{1/3}Co_{1/3}Mn_{1/3}O_2$ depends on both cation ordering in the structure and the particle size. High temperature produced $LiNi_{1/3}Co_{1/3}Mn_{1/3}O_2$ exhibit higher reversible capacity due to the reduced content of Li/Ni intermixing. The nano-sized $LiNi_{1/3}Co_{1/3}Mn_{1/3}O_2$ is not suitable for long-time cycling because its poor structural stability and increased surface area both accelerate the capacity fading. In addition, the nano-sized $LiNi_{1/3}Co_{1/3}Mn_{1/3}O_2$ does not show its advantage for rate performance because the cation disorder limits its rate capability. When the particle size becomes very big, it becomes the dominant factor that limits the rate capability. Therefore to further improve the electrochemical performance of $LiNi_{1/3}Co_{1/3}Mn_{1/3}O_2$ cathode material, a strategy that can produce nano-sized $LiNi_{1/3}Co_{1/3}Mn_{1/3}O_2$ with small amount of cation disorder is imperative.

Acknowledgements

This research is supported by National University of Singapore, Agency for Science, Technology and Research through the research grant R-265-000-292-305.

References

[1] K. Mizushima, P.C. Jones, P.J. Wiseman, J.B. Goodenough, Mater. Res. Bull. 15 (1980) 783–789.
[2] J.M. Tarascon, M. Armand, Nature 414 (2001) 359.
[3] H. Xia, S.B. Tang, L. Lu, J. Alloys Compd. 449 (2008) 296–299.
[4] W.K. Zhang, C. Wang, H. Huang, Y.P. Gan, H.M. Wu, J.P. Tu, J. Alloys Compd. 465 (2008) 250–254.
[5] Y.H. Ding, P. Zhang, Z.L. Long, Y. Jiang, D.S. Gao, J. Alloys Compd. 462 (2008) 340–342.
[6] J.J. Liu, W.H. Qiu, L.Y. Yu, H.L. Zhao, T. Li, J. Alloys Compd. 449 (2008) 326–330.
[7] B.J. Wang, Y.W. Tsai, D. Carlier, G. Ceder, Chem. Mater. 15 (2003) 3676–3682.
[8] D.C. Li, T. Muta, L.Q. Zhang, M. Yoshio, H. Noguchi, J. Power Sources 123 (2004) 150–155.
[9] B. Lin, Z.Y. Wen, Z.H. Gu, S.H. Huang, J. Power Sources 175 (2008) 564–569.
[10] S. Patoux, M.M. Doeff, Electrochem. Commun. 6 (2004) 767–772.
[11] M.H. Lee, Y.J. Kang, S.T. Myung, Y.K. Sun, Electrochim. Acta 50 (2004) 939–948.
[12] M.V. Reddy, G.V.S. Rao, B.V.R. Chowdari, J. Power Sources 159 (2006) 263–267.
[13] M. Kunduraci, J.F. Al-Sharab, G.G. Amatucci, Chem. Mater. 18 (2006) 3585–3592.
[14] W.S. Yoon, Y. Paik, X.Q. Yang, M. Balasubramanian, J. McBreen, C.P. Grey, Electrochem. Solid State Lett. 5 (2002) A263–A266.
[15] P.S. Whitfield, I.J. Davidson, L.M.D. Cramswick, I.P. Swainson, P.W. Stephens, Solid State Ionics 176 (2005) 463–471.
[16] K. Kang, Y.S. Meng, J. Breger, C.P. Grey, G. Ceder, Science 311 (2006) 977–980.
[17] T. Ohzuku, K. Nakura, T. Aoki, Electrochim. Acta 45 (1999) 151–160.
[18] H. Kobayashi, Y. Arachi, H. Kageyama, H. Sakaebe, K. Tatsumi, D. Mori, R. Kanno, T. Kamiyama, Solid State Ionics 175 (2004) 221–224.
[19] N.A. Chernova, M.M. Ma, J. Xiao, M.S. Whittingham, J. Breger, C.P. Grey, Chem. Mater. 19 (2007) 4682–4693.
[20] A.A. Ghany, K. Zaghib, F. Gendron, A. Mauger, C.M. Julien, Electrochim. Acta 52 (2007) 4092–4100.
[21] M.M. Ma, N.A. Chernova, B.H. Toby, P.Y. Zavalij, M.S. Whittingham, J. Power Sources 165 (2007) 517–534.
[22] Y.J. Shin, W.J. Choi, Y.S. Hong, S. Yoon, K.S. Ryu, S.H. Chang, Solid State Ionics 177 (2006) 515–521.
[23] J.J. Liu, W.H. Qiu, L.Y. Yu, G.H. Zhang, H.L. Zhao, T. Li, J. Power Sources 174 (2007) 701–704.
[24] H. Xia, L. Lu, Y.S. Meng, G. Ceder, J. Electrochem. Soc. 154 (2007) A337–A342.
[25] A. Van der Ven, G. Ceder, Electrochem. Commun. 6 (2004) 1045–1050.
[26] J. Breger, Y.S. Meng, Y.Y. Hinuma, S. Kumar, K. Kang, Y.S. Horn, G. Ceder, C.P. Grey, Chem. Mater. 18 (2006) 4768–4781.
[27] J. Choi, A. Manthiram, Electrochem. Solid State Lett. 8 (2005) C102–C105.
[28] D. Aurbach, B. Markovsky, A. Rodkin, E. Levi, Y.S. Cohen, H.J. Kim, M. Schmidt, Electrochim. Acta 47 (2002) 4291–4306.
[29] Z.H. Chen, J.R. Dahn, Electrochim. Acta 49 (2004) 1079–1090.